Materials Advances

ROYAL SOCIETY OF CHEMISTRY

PAPER

View Article Online
View Journal | View Issue

Cite this: *Mater. Adv.*, 2023, 4, 3207

PEGylated poly(lactic-*co*-glycolic acid) nanoparticles doped with molybdenum-iodide nanoclusters as a promising photodynamic therapy agent against ovarian cancer†

Alexis Verger, *[a] Gilles Dollo,[ab] Nolwenn Brandhonneur,[a] Sophie Martinais,[a] Stéphane Cordier,[a] Kamil Lang,[c] Maria Amela-Cortes[a] and Kaplan Kirakci *[c]

Received 2nd May 2023,
Accepted 26th June 2023

DOI: 10.1039/d3ma00206c

rsc.li/materials-advances

Photodynamic applications requires efficient intracellular uptake of the photosensitizer that can be achieved through the development of nanoscaled delivery system. Herein, we prepared PEGylated poly(lactic-*co*-glycolic acid) nanoparticles doped with an octahedral molybdenum cluster complex bearing iodine inner ligands and *o*-carborane carboxylate apical ligands. This complex is a potent red luminophore and singlet oxygen photosensitizer under UV/blue-light irradiation, making it an attractive theranostic tool for photodynamic therapy and emerging modalities such as X-ray-induced photodynamic therapy or boron neutron/proton capture therapy. However, its hydrophobicity hinders its use in biological application and requires its encapsulation in nanocarriers. The nanoparticles, prepared using the solvent displacement method, displayed ideal properties in terms of size and zeta potential as a drug delivery system and exhibited a robust colloidal stability in biological medium, without the need of additional surfactant. The encapsulated complexes conserved their efficient red luminescence and singlet oxygen photosensitizing activity, while being protected from the detrimental hydrolysis process generally observed for this type of complexes in aqueous media. Evaluation of the *in vitro* biological activity of the nanoparticles against the ovarian cancer cell line SKOV-3 evidenced efficient uptake into the cellular membrane and cytoplasm and intensive phototoxic effect associated with an appreciable therapeutic window, suggesting potential as a photodynamic therapy agent against ovarian cancer.

Introduction

Photodynamic therapy (PDT) is a minimally invasive procedure allowing to treat various conditions going from actinic keratosis to shallow-seated tumors.[1] Its therapeutic effect is based on the activation by light of a photosensitizer which transfer the absorbed energy to molecular oxygen to form the highly reactive singlet oxygen. Among the possible photosensitizers, octahedral molybdenum cluster (Mo_6) complexes have recently demonstrated their relevancy in the context of PDT. These complexes, denoted $[\{Mo_6L^i_8\}L^a_6]^n$, are formed of an octahedron of molybdenum atoms surrounded by eight inner ligand (L^i) and six inorganic or organic apical ligands (L^a). Upon excitation with UV/blue light up to approximately 550 nm, they from long lived triplet states that relax *via* a red-NIR phosphorescence.[2] In the presence of oxygen, these triplet states are quenched by molecular oxygen to form the highly reactive singlet oxygen, $O_2(^1\Delta_g)$, with high quantum yields.[3,4] In addition these complexes do not suffer from self-quenching of their luminescent properties in the aggregated state like common photosensitizers such as porphyrins, which allows their use at high concentrations in materials. These properties have led to various applications in PDT,[5–12] X-ray induced PDT,[13–16] or photoinactivation of bacteria.[17–20]

Direct administration of Mo_6 complexes is not pertinent for photodynamic applications owing to their instability in aqueous medium which results in the displacement of apical ligands by water molecule. This generally leads to aggregation and worsening of the photosensitizing and cellular uptake properties. Hydrolysis can be mitigated by the use of bulky hydrophobic apical ligands such as diphenylphosphinate.[6] However, this leads to poor water solubility of the complexes thus limiting their cellular uptake. Nanoparticles have been engineered and

[a] *Univ Rennes, ISCR (Institut des Sciences Chimiques de Rennes) – UMR 6226, F-35000, Rennes, France. E-mail: alexis.verger@univ-tours.fr*
[b] *CHU de Rennes, Pôle Hospitalo-Universitaire de Pharmacie, F-35033, Rennes, France*
[c] *Institute of Inorganic Chemistry of the Czech Academy of Sciences, Řež 1001, 250 68 Husinec-Řež, Czech Republic. E-mail: kaplan@iic.cas.cz*

† Electronic supplementary information (ESI) available. See DOI: https://doi.org/10.1039/d3ma00206c

applied for insoluble bioactive compounds by improving their aqueous solubility, their pharmacokinetics, their bioavailability and by reducing their toxicity.[21] Natural or synthetic polymers are particularly attractive as colloidal nanocarriers for the delivery of a wide variety of therapeutic molecules for cancer treatment.

In this respect, the biocompatible and biodegradable poly(lactic-*co*-glycolic acid) (PLGA) is a prolific synthetic polymer approved to produce drug delivery systems combining high payload, controlled drug release, and tumor-targeting.[22] PLGA nanoparticles have demonstrated enhanced cellular internalization and toxicity of drugs such as curcumin and kaempferol on cisplatin resistant ovarian cells line when compared to free drugs.[23,24] Despite these many advantages, clinical use of PLGA nanoparticles can be hampered by their rapid elimination from the circulation *via* the reticuloendothelial system (RES). In addition, the use of surfactant is usually necessary in the therapeutic formulation to reach a good colloidal stability. PEGylation of nanoparticles can significantly reduce the uptake by RES and increase their circulatory half-time, as well as providing high colloidal stability in biological medium.[25]

In this study a di-block copolymer poly(ethylene glycol) methyl ether-*block*-poly(lactic-*co*-glycolic) (PLGA–PEG) was used to encapsulate the cluster compound $Na_2[\{Mo_6I_8\}(1\text{-OCO-}1,2\text{-}C_2B_{10}H_{11})_6]$ (**1**) (Fig. 1). This compound displays high luminescence and singlet oxygen quantum yields and its high content of heavy atoms and boron atoms make it attractive for alternative therapeutic modalities such as X-ray-induced PDT or boron neuron/proton capture therapy.[26] However, its hydrophobicity constitutes an obstacle to its use in biological applications requiring its encapsulation in nanocarriers. The morphology as well as the colloidal and hydrolytic stability and the photosensitizing ability of the **1@PLGA–PEG** nanoparticles in phosphate-buffered saline solution (PBS) were investigated by means of transmission electron microscopy (TEM), dynamic light scattering (DLS) and luminescence spectroscopy. *In vitro* biological experiments on SKOV-3 ovarian cancer cells evidenced high photodynamic efficiency associated with efficient uptake of the nanoparticles and ROS production.

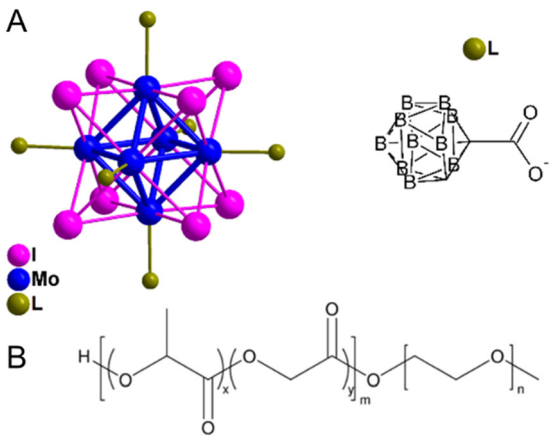

Fig. 1 Schematic representation of the components of the cluster-doped nanoparticles. (A) $[\{Mo_6I_8\}L_6]^{2-}$ cluster complexes with corresponding apical ligands (L: *o*-carborane carboxylate). (B) Poly(ethylene glycol)methyl ether-*block*-poly(lactic-*co*-glycolic) (PEG average molecular weight 5000 g mol^{-1}, PLGA average molecular weight 20 000 g mol^{-1}, lactic : glycolic 50 : 50).

Results and discussion

Preparation and characterization

1@PLGA–PEG was prepared by the solvent displacement method, in a similar way as previously reported.[9–11] In brief, an acetone solution of **1** and PLGA–PEG (PEG average molecular weight 5000 g mol^{-1}, PLGA average molecular weight 20 000 g mol^{-1}, lactic:glycolic 50 : 50) was added dropwise to a water saline solution under magnetic stirring. The use of water saline solution instead of deionized water prevents the osmotic shock occurring upon transfer of the colloidal suspension of the nanoparticles to PBS/culture medium. The acetone was removed on a rotary evaporator and the resulting colloidal suspension was centrifuged in order to get rid of big aggregates. The suspension was then stored in the fridge at 4 °C for further characterizations. Transmission electron microscopy of the colloidal suspension evidenced nanoparticles with a diameter of 47 ± 9 nm, seemingly composed of a core containing heavy elements (*i.e.*, Mo_6 complexes), surrounded by a shell made of lighter elements (*i.e.*, PLGA–PEG) (Fig. 2).

Dynamic light scattering measurement in PBS revealed nanoparticles with a mean diameter by number of 70 ± 20 nm and an almost neutral zeta potential which are advantageous features for a drug delivery system (Table 1 and Fig. S1, ESI†). Note that under similar conditions, bare **1** forms large aggregates, unmeasurable by DLS. One-week old PBS dispersions of the **1@PLGA–PEG** nanoparticles displayed comparable size distribution and zeta potential, indicating long term colloidal stability and no detectable leakage of the cluster, which would lead to the formation of large aggregates.[8] Thus the PEG moieties provides high colloidal stability to the nanoparticles without the use of a surfactant which can lead to detrimental cytotoxic effects.

The photophysical properties of the nanoparticles were studied in PBS, a relevant medium for biological applications and are summarized in Table 2. The absorption spectra of a PBS dispersion of **1@PLGA–PEG** displayed typical features of Mo_6 complexes with broad absorption bands in the UV-A/blue

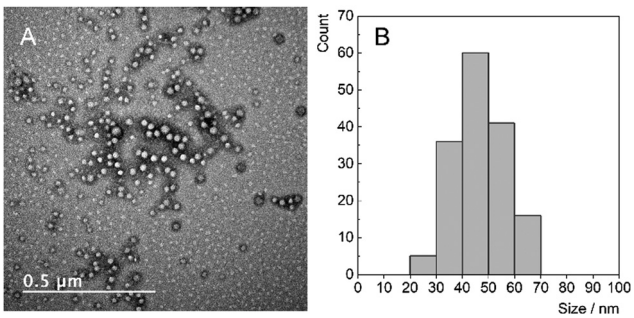

Fig. 2 Transmission electron microscopy image of **1@PLGA–PEG** (A) and corresponding particle size distribution (B).

Table 1 Size distributions and zeta potentials of fresh and one-week old PBS dispersions of **1@PLGA–PEG** at room temperature, as obtained by dynamic light scattering

Sample	Number mean/nm	*Z*-average/nm	PDI	Zeta potential/mV
1@PLGA–PEG[a]	70 ± 20	103	0.11	−1.7 ± 1.0
1@PLGA–PEG[b]	75 ± 20	104	0.12	−1.8 ± 1.0

[a] Fresh PBS dispersion. [b] 1-Week old PBS dispersions kept at room temperature.

Table 2 Photophysical properties of **1** and **1@PLGA–PEG** in PBS at room temperature[a]

Sample	λ_L/nm	τ_L/μs	τ_{air}/μs	Φ_L
1	685 (720[c])	205[b]	15[b] (15[bc])	0.55
1@PLGA–PEG	680 (680[c])	258	67[b] (71[bc])	0.68

[a] λ_L – emission maximum (λ_{exc} = 400 nm); τ_L and τ_{air} – amplitude average phosphorescence lifetimes in oxygen-free and air-saturated PBS, respectively (λ_{exc} = 405 nm, λ_{em} = 700 nm,); Φ_L – phosphorescence quantum yields in oxygen-free solutions, respectively (λ_{exc} = 320–400 nm, experimental error of Φ_L is ± 0.01). [b] Biexponential decay. [c] After 1 week in PBS at room temperature.

region (Fig. S2, ESI†). Upon light irradiation at 400 nm, the PBS dispersion displayed the characteristic red phosphorescence of the cluster complexes with maxima at 680 nm (Fig. 3A). A remarkably high phosphorescence quantum yield of 0.68 was measured for **1@PLGA–PEG**, with a corresponding long lifetime of 258 μs. In the presence of oxygen, the triplet states were efficiently quenched as evidenced by the decrease of the phosphorescence intensity and shorter lifetime in air atmosphere of 67 μs respectively (Fig. 3B). For comparison, bare **1** displayed slightly red-shifted emission maximum, lower emission quantum yield but more efficient oxygen quenching of the emission, highlighting the effect of the polymeric matrix on the photophysical properties (Table 2 and Fig. S3, ESI†) The production of $O_2(^1\Delta_g)$ was directly demonstrated by measuring its near infrared phosphorescence centred at 1274 nm (Fig. 3C).

Hydrolysis of the Mo_6 complexes is generally connected with a bathochromic shift of the emission maximum and a decrease of the emission intensity and lifetime.[5–7] When compared with a fresh one, 1 week old PBS dispersion of the nanoparticles showed almost unchanged emission maximum and emission lifetime while the emission maximum of bare **1** shifted to 720 nm due to hydrolysis of the cluster complexes, evidencing the protective effect of the PLGA–PEG nanocarrier (Fig. S4 and S5, ESI† and Table 2).

Cellular uptake and *in vitro* cytotoxicity

The human ovarian cancer cell line, SKOV-3, was chosen for the biological evaluation. Indeed, ovarian cancer is a good target for photodynamic treatment as suggested in several recent studies.[27] Uptake of the Mo_6-doped nanoparticles was monitored using confocal laser scanning microscopy. As illustrated in Fig. 4, an efficient cellular uptake of **1@PLGA–PEG** was observed characterized by a uniform distribution of the nanoparticles within the cytoplasm, as well as colocalization of the nanoparticles with the cell membrane.

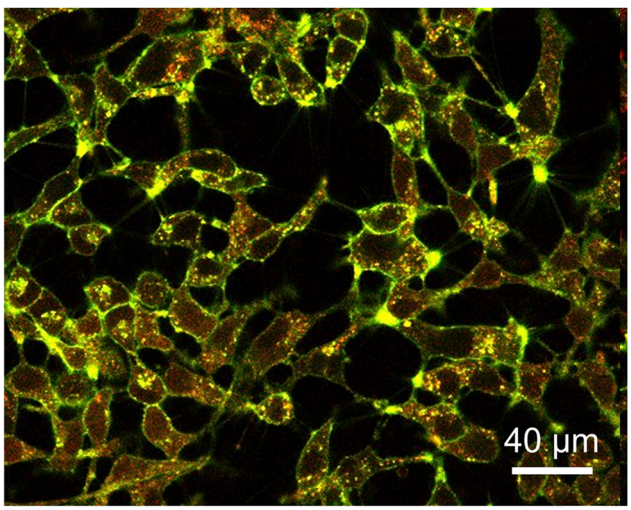

Fig. 4 Localization of **1@PLGA–PEG** in SKOV-3 cells. Confocal sections showing localization of the Mo_6-doped-doped nanoparticles (red) within the cytoplasm and colocalization (yellow) with the cellular membranes, stained with fluorescein isothiocyanate-labeled wheat germ agglutinin (green).

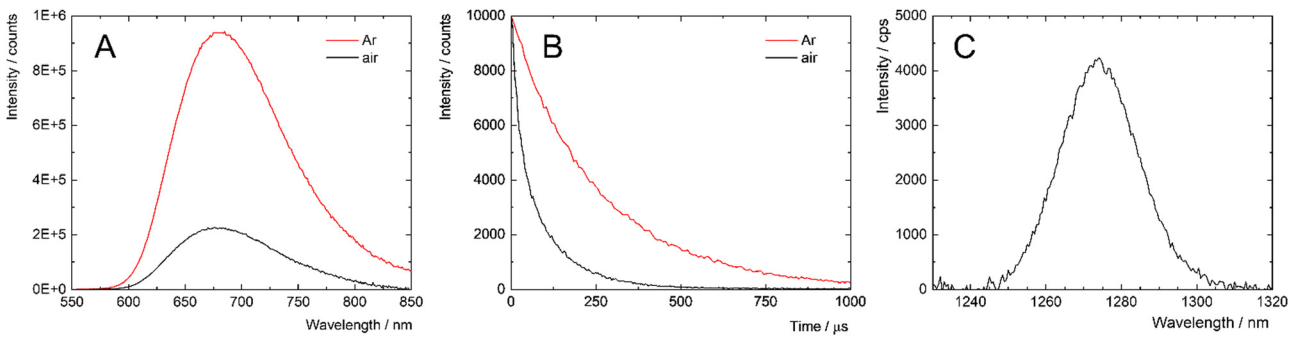

Fig. 3 Phosphorescence emission spectra of **1@PLGA–PEG** (A) in argon (red) and air (black) saturated PBS, excited at 400 nm. Phosphorescence decay kinetics at 700 nm of **1@PLGA–PEG** (B) in argon (red) and air (black) saturated PBS, excited at 405 nm. Phosphorescence signal of $O_2(^1\Delta_g)$ produced by **1@PLGA–PEG** (C) in oxygen saturated PBS, excited at 400 nm.

Table 3 IC_{50} obtained for **1@PLGA–PEG** on SKOV-3 and A2780 cells, not activated (IC_{50}) and photo-activated (IC_{50} PA). Each value is the mean ± S.D. of > 10 determinations[a]

Cell line	IC_{50} (μM)	IC_{50} PA (μM)
SKOV-3	9.00 ± 0.46	0.87 ± 0.14
A2780	9.13 ± 0.42	0.78 ± 0.12

[a] After 24 h incubation; irradiation at 365 nm for 10 min.

The cellular viability on SKOV-3 cells was determined following 24 h incubation for non-activated (*i.e.*, dark experiments) **1@PLGA–PEG** using the MTT assay at relevant concentration of clusters ranging from 0.25 to 50 μM. Table 3 indicates IC_{50} values for **1@PLGA–PEG** on SKOV-3 cells obtained from cellular viability experiment. As seen in Fig. 5A, **1@PLGA–PEG** was not toxic at clusters concentrations up to 5 μM (viability > 80%), in adequation with previously reported Mo_6-doped PLGA nanoparticles.[9–11] The cellular viability obtained for non-activated Mo_6-doped nanoparticles decreased with increasing cluster concentrations leading to an IC_{50} value of 9.00 ± 0.46. (Fig. 5B and Table 3). For comparison, an IC_{50} value of 9.13 ± 0.42 was obtained for the A2780 ovarian cancer cell line.

Previous works evidenced strong phototoxic activity of Mo_6 complexes as molecular photosensitizers.[5–7] Moreover, phototoxic experiments are a good starting point towards the use of alternative form of excitation such as ionizing radiations. Indeed, previously reported Mo_6-based nanoparticles, efficient for X-PDT, displayed also high phototoxicity.[13,15] Thus, the photodynamic toxicity of the nanoparticles upon light irradiation a 365 nm was evaluated by the MTT assay after 5 h incubation time. A strong photo-toxicity was evidenced for **1@PLGA–PEG** with IC_{50} value of 0.87 ± 0.14 μM (Fig. 5A and Table 3). The phototoxicity on another ovarian cancer cell A2780 was comparable with an IC_{50} value of 0.78 ± 0.12 μM (Fig. 5B and Table 3) suggesting a homogeneous behavior of the nanoparticles against different ovarian cancer cell lines and an appreciable therapeutic window. The measured IC_{50} value for photo-activated for **1@PLGA–PEG** was among the lowest for Mo_6-based delivery systems[9–11] and inferior to that of common photosensitizers such as temoporfin (IC_{50} > 2.5 μM) or typical chemotherapy agents such as cisplatin (IC_{50} > 1.5 μM).[9,23,24,28,29]

Biological activity on human ovarian cancer cell line SKOV-3

When the photo-activation occurs in the presence of oxygen, Mo_6 complexes act as powerful photosensitizers, generating ROS efficiently, demonstrating their usability in PDT of cancer cells. The activation of internalized Mo_6 within cells initiates oxidative stress by liberation of reactive oxygen species such as $O_2(^1\Delta_g)$, responsible for cellular death *via* necrosis pathway or *via* interaction with cellular components and initiation of apoptosis signaling.[30–32] Thus, the apoptosis inducing properties of the Mo_6-doped nanoparticles were investigated by staining with fluorescein isothiocyanate-labelled annexin V/propidium iodide (annexin V-FTIC/PI). Necrosis could be differentiated by simultaneous staining with PI who can bind to the cellular DNA in cells where the cell membrane has been totally compromised.[33] We use Hoechst 33 342 to dye DNA (even if it is damaged), to count every cells. Thus, it was possible to obtain the relative percentages of necrosis *vs.* apoptosis *vs.* healthy cells. The histograms from SKOV-3 cells treated with **1@PLGA–PEG** at 0.5 and 1 μM for 24 h were compared to that of the control experiment without nanoparticles (Fig. 6A). The **1@PLGA–PEG** nanoparticles induced dominantly necrosis in the SKOV-3 cell line at the studied concentrations.

The intracellular production of ROS was evaluated using the 2′,7′-dichlorofluorescein diacetate probe (DCF-DA), a chemically reduced form of fluorescein commonly used as a luminescent indicator of intracellular oxidative stress. The cells were incubated at non-toxic concentrations of 1, 2 and 5 μM of **1@PLGA–PEG** and then light-irradiated. Measurement of the relative fluorescence intensity of the oxidized probe evidenced a dose-dependent ROS production (Fig. 6B). Indeed, at 1 and 2 μM, the production of ROS appeared to be rather weak and comparable to that of the negative control (*i.e.*, cells incubated only with medium). On the other hand, at 5 μM, the ROS production was equivalent to that of 50 μM incubation concentration of H_2O_2, used as a positive control. It is surprising that no significant ROS production was evidenced at 1 and 2 μM of

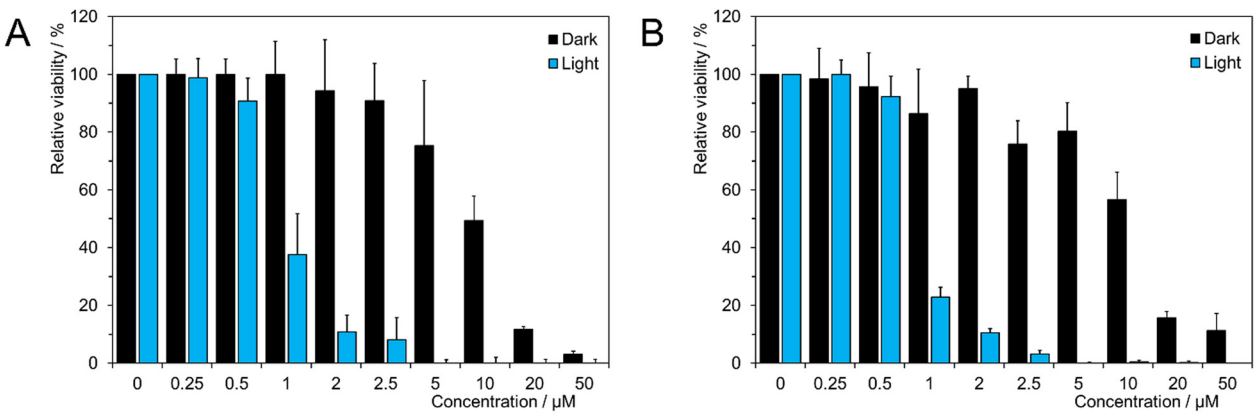

Fig. 5 Cellular viability of SKOV-3 (A) and A2780 (B) after 5 h incubation with **1@PLGA–PEG**, then left in the dark (black) or irradiated at 365 nm for 10 min (blue). Afterwards, cells were re-incubated for a 24 h period.

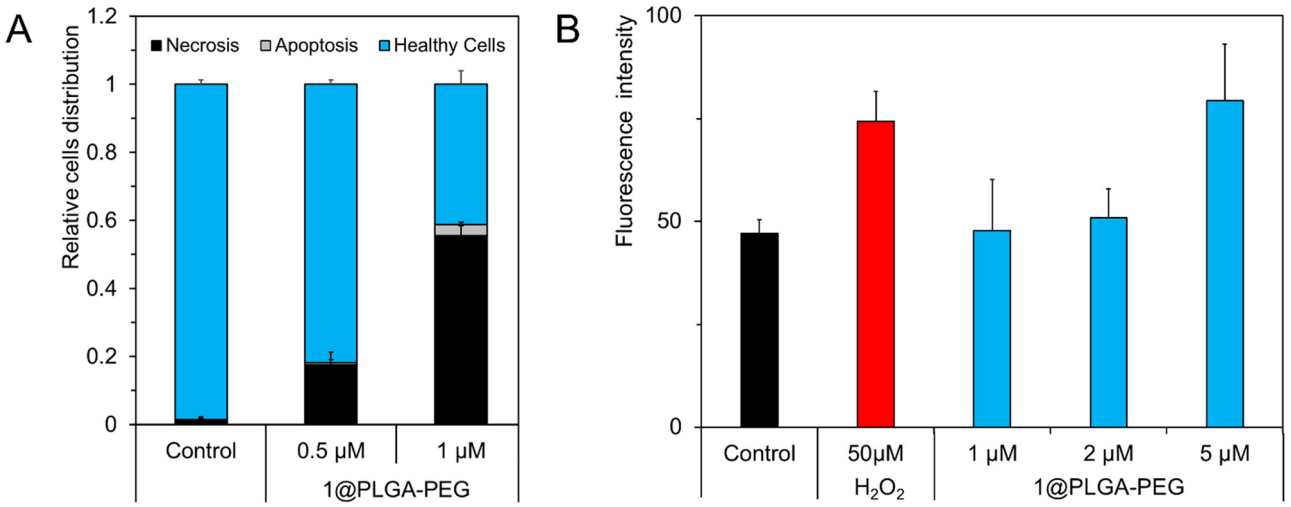

Fig. 6 (A) Cellular distribution (healthy, apoptotic or necrotic cells) following irradiation at 365 nm of SKOV-3 cells incubated with 0.5 and 1 μM of **1@PLGA–PEG**. (B) ROS production following irradiation at 365 nm of SKOV-3 incubated with 1, 2 and 5 μM of **1@PLGA–PEG** (blue). Black bar represents the negative control experiment with SKOV-3 cells incubated only with medium. Red bar represents the positive control experiment with SKOV-3 cells incubated with 50 μM of H_2O_2.

1@PLGA–PEG, concentrations that provides an evident phototoxic effect. This feature suggests that an alternative pathway to cell death could be at play. Thus, high-throughput image analysis was used to evaluate the ability of clusters-loaded nanoparticles to modify DNA, as this process was previously evidenced for a comparable Mo_6-based nanosystem.[11] The results showed that no significant DNA damage was observed for SKOV-3 cells incubated with concentrations of **1@PLGA–PEG** up to 10 μM (Fig. S6, ESI†). Thus, it is unclear why the phototoxicity of the nanoparticles is not accurately reflected by the analysis of photoinduced ROS production or DNA damage and further studies are needed in order to explain this discrepancy. Nevertheless, a possible explanation could be a different sub-cellular localization of the nanoparticles and the probes which could result in lower sensitivity of the probe to ROS produced by the nanoparticles.

Materials and methods

Reagents and general procedures.

Compound $Na_2[\{Mo_6I_8\}(1\text{-OCO-}1,2\text{-}C_2B_{10}H_{11})_6]$ (**1**) was prepared according to previously published procedure.[26] Poly(ethylene glycol)methyl ether-*block*-poly(lactic-*co*-glycolic) (PEG average molecular weight 5000 g mol^{-1}, PLGA average molecular weight 20 000 g mol^{-1}, lactic : glycolic 50 : 50), sodium chloride, and phosphate-buffered saline (10× concentrate, BioPerformance Certified) (PBS) were obtained from Sigma Aldrich and used as received. Solvents for the syntheses were purchased from Penta (Czech Republic).

Images of the nanoparticles were acquired by transmission electron microscopy, using a JEOL 2100 (JEOL, Japan). The nanoparticle size distributions and corresponding zeta potentials were determined by dynamic light scattering (DLS) on a particle size analyser Zetasizer Nano ZS (Malvern, UK). UV-vis absorption spectra were measured on a PerkinElmer Lambda 35 spectrometer. Phosphorescence properties of the nanoparticles were analysed on a FLS1000 spectrometer (Edinburgh Instruments, UK) using a cooled PMT-900 photon detection module (Edinburgh Instruments, UK). Aqueous dispersions of the nanoparticles (0.1 mg mL^{-1}) were saturated with air or argon to assure different oxygen concentrations for phosphorescence analyses. The FLS1000 spectrometer was also used for time-resolved phosphorescence measurements (λ_{exc} = 405 nm, VPLED Series) and the recorded decay curves were fitted to exponential functions by the Fluoracle software (v. 2.13.2, Edinburgh Instruments, UK). Phosphorescence quantum yields of the samples were recorded using a Quantaurus QY C11347-1 spectrometer (Hamamatsu, Japan). Singlet oxygen phosphorescence was measured on a on a Fluorolog 3 spectrometer using a Hamamatsu H10330-45 photomultiplier. In this case, aqueous dispersions of identical absorbance were saturated with oxygen to magnify the phosphorescence signal of singlet oxygen.

Preparation of 1@PLGA–PEG

2 mg of **1** and 4 mg of PLGA–PEG were dissolved in 400 μL of acetone. The resulting solution was added dropwise to 2 mL of water saline solution (NaCl, 9 g L^{-1}). Then, acetone was removed on a rotary evaporator (30 °C, 200 mbar, 60 min). The resulting colloidal suspension was centrifuged at 2000 rpm for 5 min in order to remove big aggregates and stored at 4 °C for further experiments.

Cellular studies

Cell culture. The ovarian cell carcinoma lines, SKOV-3 and A2780, were purchased from Sigma (Sigma Aldrich, France). Cells were cultured in Dulbecco's Modified Eagle Medium (DMEM) for SKOV-3 cells and supplemented with 10% fetal bovine serum (FBS) and 1% (v/v) penicillin/streptomycin under

a humidified atmosphere (5% CO_2 and 95% air) at 37 °C. Cells were cultured in 75 cm^2 Nunclon EasYFlask (Thermo Fisher Scientific, Waltham, USA).

Cellular viability and phototoxicity studies. SKOV-3 and A2780 cells were seeded into 96-well plates at a density of 20 000 cells per well and cultured for 24 h. Then, the cells were then washed with phosphate buffer (PBS) and freshly prepared cluster-doped nanoparticles were diluted with FBS-free medium at different cluster's concentrations of **1** (0.25, 0.5, 1, 2, 2.5, 5, 10, 20 and 50 μM). After 5 h of incubation, the cells were then activated at 365 nm for 10 min using a single-tube UV irradiation lamp (Vilber Lourmat, Collégien, France) with a power of 6 W and an irradiance of 0.61 mW cm^{-2}. In parallel, a control plate was kept in the dark. Afterwards, cells were re-incubated for a 24 h period. Untreated cells (negative control) were considered to have 100% viability and 20% DMSO treated cells (positive control) were considered to have 0% viability. The cellular viabilities were determined using the 3-(4,5-dimethylthiazol-2-yl)-2,5 diphenyltetrazolium bromide (MTT) assay. The tetrazolium ring is reduced to formazan by mitochondrial succinate dehydrogenase of active living cells. Formazan forms a precipitate in the mitochondria that is proportional to the amount of living cells (but also to the metabolic activity of each cell). MTT was added to cells at concentration of 0.2 mg mL^{-1} for 3 h, then the cell medium was removed and 200 μL DMSO were added to dissolve formazan crystals. For each well, 100 μL of formazan solution was transferred to another 96-well plate and made up to 200 μL using DMSO. Finally, cells viability was determined by reading absorbance of formazan at 560 nm using a POLARstar Optima microplate reader (BMG labtech, Ortenberg, Germany). Each concentration of the nanoparticles was tested in 5 replicates per experiment. All experiments were repeated three times in different days.

Confocal laser scanning microscopy (CLSM). SKOV-3 cells were seeded on a borosilicate slide (Lab-Tek borosilicate, 8 chambers) at a density of 25 000 cells by chamber, cultured for 72 h, then incubated for 5 h with the nanoparticles. After treatment, cells were washed twice with PBS then incubated for 10 min with fluorescein isothiocyanate-labeled wheat germ agglutinin (WGA-FITC) (Sigma) at a concentration of 1 μg mL^{-1}. Cells were imaged using a Confocal Microscope Leica DMI 6000 TCS SP8 (Leica, Wetzar, Germany). The nanoparticle phosphorescence was obtained following excitation at 365 nm and the emission signal was collected from 650 to 770 nm. WGA-FITC (Sigma) was excited at 495 nm and the fluorescence emission was collected at 519 nm.

Cellular death pathway analysis. Cellular death pathway was analyzed by the annexin V/PI assay (Annexin V-FITC Apoptosis Detection Kit, Sigma). To quantify apoptotic, necrotic and viable cells, SKOV-3 cells were seeded at a density of 35 000 cells by well into 96-well plates (Costar) and exposed to the nanoparticles for 24 h. After 5 h of incubation, one plate was activated at 365 nm for 10 min using a one-tube UV irradiation lamp (Vilber Lourmat, Collégien, France). In parallel, a control plate was kept in the dark. After overnight incubation, cells were washed twice with 37 °C warm PBS, and incubated for 10 min with 100 μL of a binding buffer containing: 0.5 μg mL^{-1} FITC-conjugated annexin V (Sigma), 2 μg mL^{-1} propidium iodide PI (Sigma) and 5 μg mL^{-1} Hoechst 33 342, nucleic acid dye for nucleus detection (Sigma). FITC-conjugated annexin V was excited at 495 nm and the fluorescence emission was collected at 519 nm. PI was excited at 535 nm and the fluorescence emission was collected at 617 nm and Hoechst 33 342 was excited at 350 nm and the fluorescence emission was collected at 461 nm. Apoptotic positive controls were treated with 0.2 μg mL^{-1} of doxorubicin hydrochloride. Image acquisition and analysis were performed using a Cellomics ArrayScan VTI/HCS Reader (ThermoScientific).

DCFH-DA assay. To monitor cellular ROS levels, SKOV-3 cells were seeded in 96-well dark plates at a density of 25 000 cells by well. A 24 h pre-incubation period allowed the cells to adhere to the bottom of the wells. After washing with PBS, the cells were incubated with 100 μL of a 20 μM solution of DCFH-DA (2′,7′-dichlorofluorescein diacetate, Sigma-Aldrich) in PBS for 45 min at 37 °C. The cells were then washed with 100 μL of PBS and then incubated with clusters loaded PLGA–PEG nanoparticles at different concentrations of (1) (1, 2 and 5 μM) in PBS. After 5 h of incubation, a plate was activated at 365 nm for 10min using a single-tube UV irradiation lamp (Vilber Lourmat, Collégien, France). Positive controls were treated with 50 μM or 200 μM of hydrogen peroxide. ROS production was measured at 20 min intervals with the POLARstar Optima microplate reader (excitation wavelength: 485 nm, emission wavelength: 520 nm).

Genotoxicity assay. SKOV-3 cells were seeded into 96-well plates at a concentration of 35 000 cells per well. The tested compounds were added when 70–80% of confluence was achieved. After 5 h of incubation, a plate was activated at 365 nm for 10 min using a single-tube UV irradiation lamp (Vilber Lourmat, Collégien, France). A control plate was kept in the dark. After 24 h incubation, genotoxicity of tested compounds was determined using the HCS DNA Damage Kit (Invitrogen, USA) according to the manufacturer's instructions. Positive controls were treated with 50 μM or 200 μM of hydrogen peroxide. DNA damage was measured by a specific antibody-based detection of phosphorylated H2AX (Ser139) in the nucleus, which is induced in response to double-strand breaks (DSB) formation. Fluorescence of Alexa Fluor® 555 secondary antibody was measured and analyzed using a Cellomics ArrayScan VTI/HCS Reader (ThermoScientific).

Statistical and pictures analysis. Results are expressed as mean values ± standard deviation (SD). The Mann–Whitney test was used for statistical analysis using the GraphPad Prism 7.0 software. The level of significance was set at $p < 0.05$. IC_{50} calculation were performed with the R software (R foundation, Austria) with the "ic50" package. Picture analyses were performed by different methods: Pearson's correlation coefficient[34,35] and Van Steensel's Cross Correlation Function (CCF)[3] with Fiji software (JACoP plugin).[36]

Conclusions

Herein, we prepared PEGylated PLGA nanoparticles doped with the octahedral molybdenum cluster compound, $Na_2[\{Mo_6I_8\}(1\text{-}OCO\text{-}1,2\text{-}C_2B_{10}H_{11})_6]$ (**1**). This compound display high luminescence and

singlet oxygen quantum yields and its high content of heavy atoms and boron atoms which make it attractive for alternative therapeutic modalities such as X-ray-induced PDT and boron neuron/proton capture therapy. The nanoparticles of approximately 50 nm in diameter formed stable colloidal suspension in PBS, thanks to the PEG functions of the polymers. Upon UV-A light irradiation, the nanoparticles display intensive red phosphorescence and produced $O_2(^1\Delta_g)$ making them useful theranostic tools for photodynamic therapy. Biological experiments against SKOV-3 ovarian cancer cell line evidenced uptake of the nanoparticles. **1@PLGA–PEG** was localized at the cell membrane and within the cytoplasm of SKOV-3 cells. The nanoparticles displayed low dark toxicity and possessed sub-micromolar IC_{50} under UV-A light irradiation against SKOV-3 ovarian cancer cell line. Overall, the presented nanosystem constitutes a promising agent for photodynamic applications. Further experiments are planned for evaluation of its efficiency using ionizing radiations as excitation source.

Author contributions

Conceptualization (G. D., N. B.), Supervision (N. B., M. C., S. C.), Investigation (A. V., K. K., S. M.), Writing – original draft (A. V., K. K.), Writing – review & editing (A. V., K. K., K. L.), Project administration (S. C., G. D., K. L.), Funding acquisition (S. C., K. L.)

Conflicts of interest

There are no conflicts to declare.

Acknowledgements

The authors are grateful to the Czech Science Foundation (No. 21-11688S) and to the Ministry of Education, Youth and Sports in the frame of Czech-French bilateral project (8J20FR008).

Notes and references

1 P. Agostinis, K. Berg, K. A. Cengel, T. H. Foster, A. W. Girotti, S. O. Gollnick, S. M. Hahn, M. R. Hamblin, A. Juzeniene and D. Kessel, *et al.*, Photodynamic therapy of cancer: An update, *Ca-Cancer J. Clin.*, 2011, **61**(4), 250–281.

2 A. W. Maverick, J. S. Najdzionek, D. MacKenzie, D. G. Nocera and H. B. Gray, Spectroscopic, electrochemical, and photochemical properties of molybdenum(II) and tungsten(II) halide clusters, *J. Am. Chem. Soc.*, 1983, **105**(7), 1878–1882.

3 K. Kirakci, P. Kubát, M. Dušek, K. Fejfarová, V. Šícha, J. Mosinger and K. Lang, A Highly Luminescent Hexanuclear Molybdenum Cluster – A Promising Candidate toward Photoactive Materials, *Eur. J. Inorg. Chem.*, 2012, (19), 3107–3111.

4 K. Kirakci, P. Kubát, J. Langmaier, T. Polívka, M. Fuciman, K. Fejfarová and K. Lang, A comparative study of the redox and excited state properties of (nBu4N)2[Mo6X14] and (nBu4N)2[Mo6X8(CF3COO)6] (X = Cl, Br, or I), *Dalton Trans.*, 2013, **42**(19), 7224.

5 K. Kirakci, J. Zelenka, M. Rumlová, J. Cvačka, T. Ruml and K. Lang, Cationic octahedral molybdenum cluster complexes functionalized with mitochondria-targeting ligands: photodynamic anticancer and antibacterial activities, *Biomater. Sci.*, 2019, **7**(4), 1386–1392.

6 K. Kirakci, J. Demel, J. Hynek, J. Zelenka, M. Rumlová, T. Ruml and K. Lang, Phosphinate Apical Ligands: A Route to a Water-Stable Octahedral Molybdenum Cluster Complex, *Inorg. Chem.*, 2019, **58**(24), 16546–16552.

7 K. Kirakci, J. Zelenka, I. Křížová, T. Ruml and K. Lang, Octahedral Molybdenum Cluster Complexes with Optimized Properties for Photodynamic Applications, *Inorg. Chem.*, 2020, **59**(13), 9287–9293.

8 K. Kirakci, M. Kubáňová, T. Přibyl, M. Rumlová, J. Zelenka, T. Ruml and K. Lang, A Cell Membrane Targeting Molybdenum-Iodine Nanocluster: Rational Ligand Design toward Enhanced Photodynamic Activity, *Inorg. Chem.*, 2022, **61**(12), 5076–5083.

9 N. Brandhonneur, T. Hatahet, M. Amela-Cortes, Y. Molard, S. Cordier and G. Dollo, Molybdenum cluster loaded PLGA nanoparticles: An innovative theranostic approach for the treatment of ovarian cancer, *Eur. J. Pharm. Biopharm.*, 2018, **125**, 95–105.

10 N. Brandhonneur, Y. Boucaud, A. Verger, N. Dumait, Y. Molard, S. Cordier and G. Dollo, Molybdenum cluster loaded PLGA nanoparticles as efficient tools against epithelial ovarian cancer, *Int. J. Pharm.*, 2021, **592**, 120079.

11 A. Verger, G. Dollo, S. Martinais, Y. Molard, S. Cordier, M. Amela-Cortes and N. Brandhonneur, Molybdenum-Iodine Cluster Loaded Polymeric Nanoparticles Allowing a Coupled Therapeutic Action with Low Side Toxicity for Treatment of Ovarian Cancer, *J. Pharm. Sci.*, 2022, **111**, 3377–3383.

12 A. O. Solovieva, Y. A. Vorotnikov, K. E. Trifonova, O. A. Efremova, A. A. Krasilnikova, K. A. Brylev, E. V. Vorontsova, P. A. Avrorov, L. V. Shestopalova and A. F. Poveshchenko, *et al.*, Cellular internalisation, bioimaging and dark and photodynamic cytotoxicity of silica nanoparticles doped by {Mo6I8}4+ metal clusters, *J. Mater. Chem. B*, 2016, **4**(28), 4839–4846.

13 K. Kirakci, J. Zelenka, M. Rumlová, J. Martinčík, M. Nikl, T. Ruml and K. Lang, Octahedral molybdenum clusters as radiosensitizers for X-ray induced photodynamic therapy, *J. Mater. Chem. B*, 2018, **6**(26), 4301–4307.

14 K. Kirakci, T. N. Pozmogova, A. Y. Protasevich, G. D. Vavilov, D. V. Stass, M. A. Shestopalov and K. Lang, A water-soluble octahedral molybdenum cluster complex as a potential agent for X-ray induced photodynamic therapy, *Biomater. Sci.*, 2021, **9**(8), 2893–2902.

15 M. Koncošová, M. Rumlová, R. Mikyšková, M. Reiniš, J. Zelenka, T. Ruml, K. Kirakci and K. Lang, Avenue to X-ray-induced photodynamic therapy of prostatic carcinoma with octahedral molybdenum cluster nanoparticles, *J. Mater. Chem. B*, 2022, **10**(17), 3303–3310.

16 T. N. Pozmogova, N. A. Sitnikova, E. V. Pronina, S. M. Miroshnichenko, A. O. Kushnarenko, A. O. Solovieva, S. S. Bogachev, G. D. Vavilov, O. A. Efremova, Y. A. Vorotnikov and

M. A. Shestopalov, Hybrid system {W6I8}-cluster/dsDNA as an agent for targeted X-ray induced photodynamic therapy of cancer stem cells, *Mater. Chem. Front.*, 2021, **5**(20), 7499–7507.

17 A. Beltrán, M. Mikhailov, M. N. Sokolov, V. Pérez-Laguna, A. Rezusta, M. J. Revillo and F. Galindo, A photobleaching resistant polymer supported hexanuclear molybdenum iodide cluster for photocatalytic oxygenations and photodynamic inactivation of Staphylococcus aureus, *J. Mater. Chem. B*, 2016, **4**(36), 5975–5979.

18 N. A. Vorotnikova, A. Y. Alekseev, Y. A. Vorotnikov, D. V. Evtushok, Y. Molard, M. Amela-Cortes, S. Cordier, A. I. Smolentsev, C. G. Burton and P. M. Kozhin, *et al.*, Octahedral molybdenum cluster as a photoactive antimicrobial additive to a fluoroplastic, *Mater. Sci. Eng., C*, 2019, **105**, 110150.

19 C. Felip-León, C. Arnau del Valle, V. Pérez-Laguna, M. Isabel Millán-Lou, J. F. Miravet, M. Mikhailov, M. N. Sokolov, A. Rezusta-López and F. Galindo, Superior performance of macroporous over gel type polystyrene as a support for the development of photo-bactericidal materials, *J. Mater. Chem. B*, 2017, **5**(30), 6058–6064.

20 K. Kirakci, T. K. N. Nguyen, F. Grasset, T. Uchikoshi, J. Zelenka, P. Kubát, T. Ruml and K. Lang, Electrophoretically Deposited Layers of Octahedral Molybdenum Cluster Complexes: A Promising Coating for Mitigation of Pathogenic Bacterial Biofilms under Blue Light, *ACS Appl. Mater. Interfaces*, 2020, **12**(47), 52492–52499.

21 S. Guo and L. Huang, Nanoparticles Containing Insoluble Drug for Cancer Therapy, *Biotechnol. Adv.*, 2014, **32**, 778–788.

22 T. Kato, C. S. Jin, H. Ujiie, D. Lee, K. Fujino, H. Wada, H. Hu, R. A. Weersink, J. Chen and M. Kaji, *et al.*, Nanoparticle targeted folate receptor 1-enhanced photodynamic therapy for lung cancer, *Lung Cancer*, 2017, **113**, 59–68.

23 M. M. Yallapu, D. M. Maher, V. Sundram, M. C. Bell, M. Jaggi and S. C. Chauhan, Curcumin induces chemo/radio-sensitization in ovarian cancer cells and curcumin nanoparticles inhibit ovarian cancer cell growth, *J. Ovarian Res.*, 2010, **3**, 11.

24 H. Luo, B. Jiang, B. Li, Z. Li, B.-H. Jiang and Y. C. Chen, Kaempferol nanoparticles achieve strong and selective inhibition of ovarian cancer cell viability, *Int. J. Nanomed.*, 2012, 3951.

25 J. V. Jokerst, T. Lobovkina, R. N. Zare and S. S. Gambhir, Nanoparticle PEGylation for imaging and therapy, *Nanomedicine*, 2011, **6**(4), 715–728.

26 K. Kirakci, V. Šícha, J. Holub, P. Kubát and K. Lang, Luminescent Hydrogel Particles Prepared by Self-Assembly of β-Cyclodextrin Polymer and Octahedral Molybdenum Cluster Complexes, *Inorg. Chem.*, 2014, **53**(24), 13012–13018.

27 H. Azaïs, J. P. Estevez, P. Foucher, Y. Kerbage, S. Mordon and P. Collinet, Dealing with microscopic peritoneal metastases of epithelial ovarian cancer. A surgical challenge, *Surg. Oncol.*, 2017, **26**(1), 46–52.

28 E. Gaio, D. Scheglmann, E. Reddi and F. Moret, Uptake and photo-toxicity of Foscan®, Foslip® and Fospeg® in multicellular tumor spheroids, *J. Photochem. Photobiol., B*, 2016, **161**, 244–252.

29 M. Altaf, N. Casagrande, E. Mariotto, N. Baig, A.-N. Kawde, G. Corona, R. Larcher, C. Borghese, C. Pavan and A. Seliman, *et al.*, Potent In Vitro and In Vivo Anticancer Activity of New Bipyridine and Bipyrimidine Gold (III) Dithiocarbamate Derivatives, *Cancers*, 2019, **11**(4), 474.

30 D. Kessel, Apoptosis, Paraptosis and Autophagy: Death and Survival Pathways Associated with Photodynamic Therapy, *Photochem. Photobiol.*, 2018, **95**(1), 119–125.

31 D. Kessel and N. L. Oleinick, Photodynamic Therapy and Cell Death Pathways, *Methods Mol. Biol.*, 2010, 35–46.

32 D. Kessel and N. L. Oleinick, Cell Death Pathways Associated with Photodynamic Therapy: An Update, *Photochem. Photobiol.*, 2018, **94**(2), 213–218.

33 A. P. Demchenko, Beyond annexin V: fluorescence response of cellular membranes to apoptosis, *Cytotechnology*, 2012, **65**(2), 157–172.

34 S. Bolte and F. P. Cordelieres, A guided tour into subcellular colocalization analysis in light microscopy, *J. Microsc.*, 2006, **224**(3), 213–232.

35 E. M. Manders, J. Stap, G. J. Brakenhoff, R. van Driel and J. A. Aten, Dynamics of three-dimensional replication patterns during the S-phase, analysed by double labelling of DNA and confocal microscopy, *J. Cell Sci.*, 1992, **103**(3), 857–862.

36 J. Schindelin, I. Arganda-Carreras, E. Frise, V. Kaynig, M. Longair, T. Pietzsch, S. Preibisch, C. Rueden, S. Saalfeld and B. Schmid, *et al.*, Fiji: an open-source platform for biological-image analysis, *Nat. Methods*, 2012, **9**(7), 676–682.